Antibodies halting motility in *Mycoplasma pneumoniae* reveal the dynamic nature of the adhesion complex

Akihiro Kawamoto[1,*], David Vizarraga[2,*], Marina Marcos-Silva[3,*], Jesús Martín[2], Fumiaki Makino[4,5], Tomoko Miyata[4,5], Jorge Roel[2], Enrique Marcos[2], David Aparicio[2], Ignacio Fita[2], Makoto Miyata[6], Jaume Piñol[3,#], Keiichi Namba[4,5,#], Tsuyoshi Kenri[7,#]

[1]*Institute for Protein Research, Osaka University, 3-2 Yamadaoka, Suita, Osaka, 565-0871, Japan.*

[2]*Instituto de Biología Molecular de Barcelona (IBMB-CSIC), Parc Científic de Barcelona, Baldiri Reixac 10, 08028 Barcelona, Spain*

[3]*Institut de Biotecnologia i Biomedicina and Departament de Bioquímica i Biologia Molecular, Universitat Autònoma de Barcelona, 08193 Cerdanyola del Vallès, Spain. Bellaterra, Spain*

[4]*Graduate School of Frontier Biosciences, Osaka University, 1-3 Yamadaoka, Suita, Osaka, 565-0871, Japan.*

[5]*JEOL YOKOGUSHI Research Alliance Laboratories, Osaka University, 1-3 Yamadaoka, Suita, Osaka, 565-0871, Japan.*

[6]*The OCU Advanced Research Institute for Natural Science and Technology (OCARINA). Osaka City University. Sumiyoshi, Osaka, Japan.*

[7]*National Institute of Infectious Diseases. Tokyo. Japan*

Abstract

Mycoplasma pneumoniae is a bacterial wall-less human pathogen and the etiological agent of atypical pneumonia and tracheobronchitis in both adults and children. *M. pneumoniae* infectivity, gliding motility and adherence to host target respiratory epithelial cells, are mediated by adhesin proteins P1 and P40/P90 forming a trans-membrane complex that binds to sialylated oligosaccharides cell receptors. Here we report the Cryo-EM structure from P1 bound to the Fab fragment of monoclonal antibody (P1/MCA4), which stops gliding and induces detachment of motile *M. pneumoniae* cells. On the contrary, polyclonal antibodies generated against the N-domain of P1 or against the whole ectodomain of P40/P90 have little or no effects on adhesion or motility. The epitope of P1MCA4, centred on loop Thr1426-Asp1438 in the small C-terminal domain of P1, is inaccessible to antibodies in the "open" conformation of the adhesion complex, when ready for attachment to sialylated oligosaccharides. Mutations in the highly conserved Engelman motifs found in the transmembrane helix of P40/P90, also alter adhesion and motility. The C-terminal domain of P1 experiences large conformational rearrangements, during the attachment/detachment cycle of the adhesion complex. These rearrangements are hindered by antibodies against the C-terminal domain interfering with gliding, which explains the specific neutralization mechanism deployed by antibodies against this domain and suggests new ways to confront *M. pneumoniae* infections.

INTRODUCTION

Mycoplasma pneumoniae (*Mycoplasmoides pneumoniae*) is a human pathogen inducing respiratory diseases and one of the leading microorganisms causing community acquired bacterial pneumonias (Waites et al., 2017). Coinfections of *M. pneumoniae* with other respiratory pathogens, such as SARS-CoV-2, Adenovirus or *Chlamydia pneumoniae*, have been associated with importantly increased morbidities (Parrott et al., 2016; Rangroo et al., 2022; Waites et al., 2017). However, the tropism for respiratory tissues of *M. pneumoniae* might be exploited for biomedical applications and attenuated strains of this mycoplasma have been recently engineered to be used as living pills to treat pulmonary diseases (Mazzolini et al., 2023).

M. pneumoniae exhibits a membrane protrusion at a cell pole, referred as the "attachment" or "terminal" organelle (TO), that is instrumental for infection and gliding motility. *M. pneumoniae* cells bind to glass surfaces coated with sialylated oligosaccharides (SOs), abundant on the human epithelial surfaces, gliding in the direction of the TO (Henderson and Jensen, 2006; Miyata and Hamaguchi, 2016; Seybert et al., 2006). The molecular machinery for motility is located in the TO and involves about fifteen different proteins organized as surface structures and internal parts (Kawamoto et al., 2016; Mizutani et al., 2021; Nakane et al., 2015). The main and most abundant surface structure is the adhesion complex known as Nap, which in *M. pneumoniae* is composed by transmembrane adhesin proteins P1 and P40/P90 (Krause et al., 1982; Scheffer et al., 2017; Vizarraga et al., 2020). Naps have an essential role in attachment to surfaces by binding to the SOs receptors (Vizarraga et al., 2021; Williams et al., 2020). The type of motility presented by *M. pneumoniae* is shared only by mycoplasma species belonging to the pneumoniae cluster (Miyata and Hamaguchi, 2016; Nakane et al., 2015).

During the last few years, several high-resolution structures have been determined for adhesins P1 and P40/P90 (Vizarraga et al., 2020) and also for the closely related orthologous proteins from *Mycoplasma genitalium* P140 and P110 (Aparicio et al., 2020, 2018). Naps were proposed to cycle between "open" and "closed" conformations where the SOs binding pockets are accessible or inaccessible, respectively. The SO binding pocket is located in the P40/P90 N-terminal domain, although accessibility to the pocket is determined by the interaction with the N-terminal domain of P1 that is tighter in the "closed" conformation.

Naps have also been named as GPCAs from "Genitalium and Pneumoniae Cyto-Adhesin" to emphasize the similar organization of Naps in both species (Mizutani et al., 2021; Vizarraga et al., 2021).

Adhesins P1 and P40/P90, together with protein P116, are the most immunogenic proteins of *M. pneumoniae* (Sprankel et al., 2023; Vizarraga et al., 2020). To study the immunogenic and functional properties of P1, monoclonal antibodies were generated against a fragment of this adhesin spanning from residue Ala1160 to Gln1518, (P1:1160-1518 peptide) (**Supplementary Table I**). One of the monoclonal antibodies obtained (henceforth referred as P1/MCA3) was reported some years ago to progressively reduce gliding speed removing mycoplasma cells from surfaces in a concentration-dependent way, while having little effect on non-moving cells (Seto et al., 2005). These observations allowed to conclude that during gliding P1 has to experience important conformational changes participating like a leg in a "power stroke" that propels the cell and where epitope exposure to antibody P1/MCA3 is significantly reduced in non-moving cells.

How the functioning of Naps relate to the motility of mycoplasma cells remains elusive. Antibody P1/MCA3 is no longer available, but we have now solved by cryo-EM the structure of P1 in complex with the Fab fragment of monoclonal antibody P1/MCA4, which was obtained at the same time that P1/MCA3 and against the same P1:1160-1518 peptide (**Supplementary Table I**). P1/MCA4 also affects motility and enhances detachment of moving mycoplasma cells similarly to P1/MCA3. The structure determined provides a snapshot of the "closed" conformation of P1 when Naps cannot attach to SOs. We also investigated how motility is affected by polyclonal antibodies against the whole ectodomains of adhesins P1 and P40/P90 and against constructs of the N-terminal domain of P1. Mutations in the highly conserved Engelman motifs, found in the transmembrane helices of adhesins, can also alter adhesion and motility, providing information about how extra- and intra-cellular regions of Naps communicate with each other. Altogether these results provide a deep inside into Nap functioning and explain the specific neutralization mechanism deployed by antibodies against the C-terminal domain of P1.

RESULTS

Monoclonal antibody P1/MCA4 and its binding to P1

Monoclonal antibody P1/MCA4, raised against the P1:1160-1518 peptide, exhibited strong hemadsorption inhibitory activity (in a 10 µg/ml concentration) for *M. pneumoniae.* In the presence of P1/MCA4, gliding mycoplasma cells reduce rapidly their speed and eventually halt and detach from (sialylated) glass surfaces (**Video I**). Non-moving cells were not affected by the presence of P1/MCA4 and remained attached to surfaces. As mentioned in the introduction, a similar behaviour had been reported for antibody P1/MCA3 (Seto et al., 2005). It is worth mention that a similar behaviour was also found for three additional monoclonal antibodies raised in the same batch as P1/MCA3 and P1/MCA4 (**Supplementary Table 1**). From the structural information now available, the P1:1160-1518 peptide contains a fragment of the N-terminal domain and the whole C-terminal domain (residues Ala1400-Asp1521).

cDNA sequencing of P1/MCA4 mRNAs in hybridoma cells, showed the presence of a single Heavy chain mRNA but two different Light chain mRNAs (**Supplementary Figure 1**). N-terminus analysis of samples from antibody P1/MCA4 (obtained as indicated in the Material and Methods) confirmed the presence of one Heavy chain but two different Light chains (roughly 70% for the most abundant). The heterogeneity of Light chains might explain in particular the failure of numerous crystallization attempts involving P1/MCA4. However, analysis by MALS showed the formation of a stable and homogeneous P1-Fab(P1/MCA4) complex in a solution with equimolecular amounts of P1/MCA4 Fabs and the whole P1ectodomain (residues Thr29-Asp1521), indicating that the two kinds of Fab found in P1/MCA4 bind efficiently to P1 (**Supplementary Figure 2**).

Antibody P1/MCA4 presented also high affinity for a construct corresponding to the C-terminal domain of P1, proving that this small domain contains the epitope (**Supplementary Figure 3a**). Moreover, western blotting analysis performed using different segments from P1, showed that residues Thr1426-Asp1438 are a key part of the epitope (**Supplementary Figure 3b**). An additional observation that could have clinical implications is that P1/MCA4 presents also affinity for the C-terminal domain of P140 (residues Lys1220-

Asp1351) from *M. genitalium*, in agreement with the high sequence and structural similarities between the C-terminal domains from *M. pneumoniae* and *M. genitalium*.

Cryo-EM structure of the P1-Fab(P1/MCA4) complex

The structure from the ectodomain of P1 bound to the Fab fragment of P1/MCA4 was determined by cryo-EM with an overall resolution of 2.4 Å (**Supplementary Figure 4** and **Supplementary Table 2**). The quality of the map allowed determining with accuracy the structure of P1 and of the Fab variable domains, defining clearly the paratope-epitope interface (**Figure 1** and **2**). The Fab constant domains were less well defined, indicating some variability in the Fab elbow. The structure of P1 consists of a large N-domain (spanning residues from 60 to 1400) and a smaller C-domain (residues 1401-1521), in full agreement with the structures from P1 reported previously (Vizarraga et al., 2020). However, superposing the P1 crystal structure (PDB code 6rc9) and the P1 structure from the P1-Fab complex, gives a root mean square deviation (rmsd) of 1.80 Å for 1236 aligned residues (from a total of 1339 in the model) (**Supplementary Figure 5**). When the superposition is done separately for the N-terminal and C-terminal domains rmsds are 1.65Å (1151 aligned residues from 1226) and 1.20Å (97 aligned from 104), respectively. These results show the high plasticity of P1, in particular for the N-terminal domain that experiences significant changes although it participates only indirectly in the interaction with the Fab. Comparison of the P1 structures, from the crystal and the P1-Fab complex, indicates a rotation of the C-terminal domain with respect to the N-terminal domain of 7.7°, confirming the feasibility of hinge movements between domains. The structure of the complex shows that the epitope of P1/MCA4 is non-linear, involving only residues from the C-terminal domain and, in particular, from loop Val1425-Asp1438 in agreement with the map epitope analysis (**Figure 1 and Supplementary Figure 3**). It is worth mentioning that the quality of the map even allowed to locate a significant number of solvent molecules in the large N-terminal domain of P1, where the local resolution is the highest (**Supplementary Figure 6**). Most of the solvent molecules found have their equivalents in the crystal structure of P1.

The ternary complex P40/P90-P1-Fab(P1/MCA4)

A solution with equimolecular amounts of Fab(P1/MCA4) and of ectodomains from P1 (residues 29-1521) and from P40/P90 (residues 23-1114) resulted in a mixture of several

complexes, where the amount of ternary complex P40/P90-P1-Fab(P1/MCA4) was small, while heterodimers P40/P90-P1 and P1-Fab(P1/MCA4) were abundant (MALS **Supplementary Figure 7)**. Checking by cryo-EM confirmed the mixture of the different complexes in 2D classifications **(Supplementary Figure 8)**. Attempts to determine the structure of the ternary complex gave a poor map with an overall resolution of *** Å, where density was missing for the C-terminal domain of P40/P90 and uninterpretable for the Fab (**Supplementary Table 3** and **Supplementary Figure 9)**. Density in the map corresponding to the C-terminal domain of P1 was quite strong, although fitting of the domain presented some ambiguity due to the limited resolution and small size of the domain. The best-defined part of the map was modeled with the N-terminal domains from P40/P90 and from P1, showing that these domains interact tightly with each other similarly to what had been determined for the "closed" structures of orthologue adhesins P110 and P140 from *M. genitalium* (Aparicio et al., 2020) (**Supplementary Figure 9**). Docking onto this model the P1-Fab structure by superimposing the N-terminal domains of P1, results in important steric clashes between the Fab and P40/P90 (**Supplementary Figure 9**), suggesting that the Fab and P40/P90 might compete with each other for the binding to P1, which explains the difficulties in obtaining the ternary complex. However, footprints of the Fab and P40/P90 when interacting with P1 do not overlap. Just a hinge rotation of the C-terminal domain from P1 allows the building of a ternary complex without steric problems (**Supplementary Figure 9**). Therefore, the low percentage of the ternary complex experimentally found indicates that the energy required by the hinge movement of the C-terminal domain from P1 is larger than the energy gained by the binding of either P40/P90 or the Fab.

Polyclonal antibodies against the P40/P90 and P1 ectodomains and against the N-terminal domains of P1

Polyclonal antisera against the ectodomains of P40/P90 (residues Ala25-Pro1113), P1(residues Thr29-Asp1521) were obtained by immunizing mice with recombinant versions of these polypeptides. Polyclonal antisera against the N-terminal domain of P1 was obtained by immunizing mice with P1 N-terminal domain (residues Thr29-Ala1375). Antisera were tested by ELISA, Western Blotting and immunofluorescence assays on whole *M. pneumoniae* cells, and titers higher than 1/2000 were obtained for all the sera (data not

shown). Effects of these antisera on *M. pneumoniae* motility and attachment were investigated by incubating *M. pneumoniae* cells and antisera in the presence (Williams et al., 2020) or in the absence (Seto et al., 2005) of 3% gelatin in SP4 medium. Because of *M. pneumoniae* cells spontaneously detach at high frequencies from the observation surface in the absence of gelatin (Sprankel et al., 2023) more reproducible and consistent results were obtained when gliding motility was analyzed in SP4 medium supplemented with gelatin. In the absence of gelatin, P1 ectodomain antisera stopped the movement of mycoplasma cells after five minutes of incubation. Stopped cells detached in a similar way as described for the P1/MCA4 monoclonal antibody. No significant effects on mycoplasma gliding were detected for the P1 N-terminal domain and the P40/P90 antisera, even at the lowest dilution tested. In the presence of gelatin and in the absence of antibodies most of the cells remained motile during the observation time. In contrast, P1 ectodomain antisera stopped the movement of mycoplasma cells in a very reproducible way after four minutes of incubation, but stopped cells did not detach from the surface (**Supplementary Videos II+ and III+ and Supplementary Table 3**). Binding of antibodies interferes with conformational transformations that alter the accessibility of epitopes. Therefore, during the Nap attachment/detachment cycle large conformational changes are expected for the C-terminal domain of P1, while the exposure of epitopes seems to remain unchanged for P40/P90 and the N-terminal domain of P1. It is also worth mention that adhesion was inhibited when cells were added to media that already contained antisera from the ectodomains of either P1 or P40/P90, sugesting that these antibodies can interfere the binding to SOs but their epitopes are not accessible when cells are attached to surfaces.

Mutations in the Engelman motifs

C-terminal domains are closely followed in the adhesins, by predicted single transmembrane helices with highly conserved sequences (**Supplementary Fig 10**). Remarkably, these helices contain one Engelman motif in P1 and two Engelman motifs in P40/P90. These motifs have the conserved sequence GXXXG, with X any residue, in general hydrophobic, and they are frequently involved in high-affinity interactions between membrane helices. We have investigated, by mutational analysis, the possible contributions of Engelman motifs to the organization and functioning of Naps. The study was performed

in *M. genitalium* because simple genetic methods to introduce point mutations are available in this microorganism and orthologues adhesins of *M. pneumoniae* and *M. genitalium* share high sequence similarities in the respective transmembrane helices (**Supplementary Fig 10**). Mutations were introduced by transposon delivery in a *M. genitalium* null mutant G37ΔAdh (G37ΔMG_191-ΔMG_192) strain, obtaining isogenic strains bearing double single-point mutations in the P140 and/or P110 Engelman otifs (henceforth referred respectively as E1 and E2, E3, see Methods and **Supplementary Table 4**). Protein profile analysis of mutant of these strains showed that adhesins bearing mutations the different Engelman motifs were expressed at similar levels than P110 and P140 WT adhesins (**Supplementary Figure 11)**. Immunolabeling with a polyclonal antiserum against the Nap complex from *M. genitalium*, showed that all the adhesin variants locate at the tip of the mycoplasma cells, as it is also found for the P110 and P140 WT adhesins (**Supplementary Figure 12)**. It had been shown that P110 and P140 adhesins complexes are essential for TO development (Burgos et al., 2006), which indicates that all the adhesin variants are properly folded, forming Nap complexes that are positioned in the TO of *M. genitalium* cells.

Adhesion properties of the different adhesin variants were tested by quantitative hemadsorption assay (**Figure 4B**). Cells from E1 mutant strain showed hemadsorption values very similar to those of WT cells. The same results were found when a WT copy of both adhesin coding genes were delivered by transposition. In contrast, E2 mutants showed an intermediate adherence phenotype and mutants from E3, at the C-end of the transmembrane helix close to the internal side of the cell membrane, showed a severely impaired hemadsorption phenotypes, characterized by low B_{max} values. We also obtained strains bearing different combinations of mutations in two of the three Engelman motifs. As expected, E1-E2 mutant strains exhibited an intermediate adherent phenotype and E1-E3 mutant strains exhibited also a severely impaired hemadsorption phenotypes. In addition, we also obtained E2-E3 and E1-E2-E3 mutant strains that showed a non-adherent phenotype characterized by unusually low B_{max} values and very high K_d values, the typical parameters of G37ΔAdh null mutant strain. These results indicate that mutations on E1 have little effects on adhesion and motility, while on the contrary Engelman motifs E2 and E3 from P110, are essential for cell adhesion. In particular, we observed a synergic effect when E2 and E3 mutations are combined, strongly suggesting that the two P110 subunits of a Nap interact

with each other throughout their Engelman motifs that are essential to achieve the "open" conformation of the Nap. On the other hand, cells from different mutant strains were also analyzed by Scanning Electron Microscopy. Cells from E1 and E2 mutants exhibited normal morphologies. In contrast, most of cells from E2-E3 and E1-E2-E3 mutants showed a multiple TO phenotype (Pich et al., 2009) and some cells from the triple mutant showed round morphologies with no detectable TOs (Supplementary Fig XX). All these results suggest that Engelman motifs from P110 are also critical for interactions of the Nap complex with cytoskeletal proteins from inner cell.

Modelling the Nap attachment-detachment cycle

Considering the results obtained in this work and the previously available information about the organization and functioning of Naps (Vizarraga et al., 2020), we have remodeled the four stages proposed for the attachment-detachment cycle of a Nap involved in gliding (Mizutani et al., 2021).

Stage I: The Nap in the "open" conformation, ready for binding to the SOs. The model of the extracellular region was built according to the structure determined "in situ" by Electron Cryo-Tomography (cryo-TEM) for the Nap in *M. genitalium* (Aparicio et al., 2020), with the structures of P1 and P40/P90 from *M. pneumoniae* replacing orthologues P140 and P110, respectively (Fig 5). Importantly, superposing onto the modeled Nap "open" conformation the structure of the P1-Fab(P1/MCA4) complex, by superposing the P1 structures, results in the catastrophic steric clash of the Fab against the adhesins, evidencing that the epitope of P1/MCA4 is totally inaccessible to antibodies in the "open" conformation of the Nap (**Fig 5i**).

Stage II: Binding to SOs triggers the transition of the Nap towards the "closed" conformation. Cooperativity in binding to sialic compounds, with Hill constants ranging from 1.5 to 2.5 determined for cells from *M. pneumoniae* and from *Mycoplasma gallisepticum* (also belonging to the pneumonia cluster of mycoplasmas), suggests that in the transition the two binding sites of a Nap are involved (Kasai et al., 2013; Mizutani and Miyata, 2019) P40/P90 ectodomains experience limited rearrangements during the transition towards the "closed" conformation, which agrees with the restrains imposed by the anchorage to SOs receptors and by the interactions between transmembrane helices from the two

P40/P90 subunits. Simultaneously, the ectodomain from P1 experiences extensive rearrangements with the C-terminal domain performing a hinge rotation that will expose the epitope of antibody P1/MCA4 and the N-terminal domain moving towards the N-terminal domain of P40/P90 (**Fig 5ii**). Rotation of the P1 C-terminal domain drags the transmembrane helix, which is contiguous in sequence with the domain (**Fig 5ii**). Therefore, conformational changes can be communicated back and forth between the extracellular and intracellular Nap regions.

Stage III: Reaching the "closed" conformation of the Nap, where N-terminal domains from P1 and P40/P90 interact tightly with each other forcing the release of SOs and occluding the binding site **(Fig 5iii)**. In the "closed" conformation the C-terminal domain and the transmembrane helix from P1 have to have completed their structural rearrangements, allowing the epitope of antibody P1/MCA4 to be fully exposed.

The unbound "closed" and "open" Nap conformations as described here until now have the same molecular components and at least one of the conformations would not be stable. Therefore, for the feasibility of the two conformations a new element is necessarily at play. Studies with *M. gallisepticum* have shown that motility was driven by ATP hydrolysis (Mizutani and Miyata, 2019). Reaching the "closed" conformation might be coupled with ADP/ATP release/binding to the Nap or to proteins interacting with the Nap.

Stage IV: Opening the "closed" conformation to recover the "open" conformation of the Nap. Opening requires, in particular repositioning back the transmembrane helix and the C-terminal domain of P1. Antibody P1/MCA4 hinders the transition towards the "open" conformation by trapping the C-terminal domain from the "closed" conformation of the Nap where the SO binding site is not accessible. Stage IV completes the attachment/detachment cycle of a Nap and, just from general thermodynamic considerations, an input of energy is required at some point of the cycle. Opening the "closed" conformation of the Nap might be driven by the intracellular hydrolysis of an ATP molecule (Fig 5iv.

DISCUSSION

M. pneumoniae infectivity, gliding motility and adherence to host target respiratory epithelial cells, are mediated by adhesion proteins P1 and P40/P90 forming the transmembrane adhesion Nap complex that binds to SOs receptors. Naps involved in the attachment-detachment cycle of moving mycoplasma cells have been proposed to adopt alternatively "open" and "closed" conformations where the SO binding sites are accessible and inaccessible, respectively. The sialic binding site is located in the N-terminal domain of P40/P90, but accessibility to the site is determined by the interactions of the N-terminal domain from P1 with P40/P90 (Aparicio et al., 2020). Binding of monoclonal antibody P1/MCA4 (corresponding to clone 4, the only presently available from the ones described in **Supplementary Table 1**) to *M. pneumoniae* cells affects just to motile cells, progressively decreasing gliding speed and inducing detachment of halted cells, as it was reported by (Seto et al., 2005).

The structure of the complex from P1 and the Fab fragment from P1/MCA4, determined here, shows a structural epitope, centred around loop Thr1426-Asp1438, that involves residues from the C-terminal domain of P1 only. This epitope is buried and totally inaccessible to antibodies in the "open" conformation of the Nap determined "in situ" for *M. genitalium.* Therefore, for the P1/MCA4 epitope to be exposed the C-terminal domain of P1 has to experience a major rearrangement with respect to the "open" configuration of the Nap. This alternative configuration corresponds to the "closed" configuration of the Nap, in agreement with the observation that only moving cells detach when exposed to the antibody. Binding of antibody P1/MCA4 to the C-terminal domain prevents the rearrangement of the domain trapping the Nap in the "closed" conformation, consequently interfering with adhesion and motility in an efficient neutralization mechanism.

Polyclonal antibodies generated against the N-terminal domain of P1 or against the whole ectodomain of P40/P90 have no effect (or very little) in the motility of cells attached to surfaces, which indicates that exposure of epitopes in these regions are not altered during the Nap cycle. However, these epitopes are exposed to when cells are free in suspension allowing that these polyclonal antibodies might block adhesion, likely because antibodies bound near the SOs binding sites block the accessibility to the SO receptors. Altogether these results, give a strong support to the idea that essentially only the C-terminal domain of P1

(and maybe also residues from the cytoadherence peptide) experiences large rearrangements, mainly hinge movements, during the attachment-detachment cycle of the Nap.

Attempts to form the ternary complex P1-P40/P90-Fab(P1/MCA4) gave a mixture where the binary complexes P1-Fab(P1/MCA4) and, in particular, P1-P40/P90 are the most abundant species. Docking Fab(P1/MCA4) onto the P1-P40/P90 complex results in important steric clashes between the Fab and the N-terminal domain of P40/P90, which explains the difficulties in obtaining the ternary complex. These steric clashes would be eliminated by a hinge rearrangement of the C-terminal domain of P1 similar to the one proposed to occur during the transitions between the "open" and "closed" states of the Nap. Difficulties in forming this ternary complex indicate that the rearrangement of the C-terminal domain is energetically costly. Therefore, transitions in the Nap ectodomains are the result of a balance between the preferred conformations of the C-terminal domains of P1, favouring the "open" configuration of the Nap, and the preferred interactions between the N-terminal domains of P1 and P40/P90, favouring the "closed" state. "In vivo" structural changes in the Nap ectodomains, in particular in the C-terminal domain of P1, will communicate back and forth with intra-cellular regions throughout the displacements of trans-membrane helices contributing also to the global balance between the different conformations of the Nap.

In a recent study of forces involved in gliding, it was proposed that each Nap contributes to both attachment and movement in a gliding scheme composed of four stages connected by four steps with Naps having a key role in each step (Mizutani et al., 2021). The proposal was a new variant of the "inchworm" model, in which repeated extensions and contractions, synchronized with alternative attachment and detachment of the TO front and rear sides, enable the smooth gliding of cells (Henderson and Jensen, 2006; Miyata, 2008; Seybert et al., 2018). Rearrangements and the extra-/intra-cellular communication of the Nap during the attachment/detachment cycle now determined provides a consistent structural framework for this variant of the inchworm model, in which adhesin P1 experiences extensive rearrangements pivoting around a (mostly) fixedP40/P90. Results obtained in this work provide a deeper inside into the role of the Nap during gliding explaining in particular, how antibodies directed against the highly conserved but highly dynamic C-terminal domain of P1, block very effectively the attachment/detachment cycle suggesting new approaches to confront pathogens from the pneumonia cluster of mycoplasmas.

Experimental Procedures

Bacterial strains and tissue culture cells

M. pneumoniae M129 strain was grown in cell culture flasks containing SP4 or PPLO media and incubated at 37 ºC with or without 5% CO_2. Surface-attached mycoplasmas were harvested using a cell scraper and resuspended in medium or suitable buffers for experiments. When growing mycoplasma cells on IBIDI 8-well chamber slides, each well was seeded with about 10^5 CFUs and incubated for 12-24 h in 200 µL SP4 supplemented with 3% gelatin. All *M. genitalium* strains (**Supplementary Table X)** were grown in SP-4 broth at 37°C in a 5% CO_2 atmosphere in tissue culture flasks. SP-4 plates were prepared supplementing the medium with 0.8% agar (BD). Chloramphenicol (17 µg ml^{-1}), puromycin (3 µg ml^{-1}) or gentamycin (100µg ml^{-1}) were added for mutant selection.

Escherichia coli strain XL-1 Blue (Agilent, Santa Clara, USA) was used for cloning and plasmid propagation purposes. The strain was grown in Luria Bertani (LB) or LB agar plates containing 100µgml^{-1} ampicillin, 40µgml^{-1} X-Gal, and 24µgml^{-1} Isopropyl β-D-1-thiogalactopyranoside (IPTG) when needed.

NSI myeloma cells (Köhler and Milstein, 2005)(Köhler & Milstein, 2005) were grown in RPMI 1640 medium supplemented with 10% FBS and 50 µg mL^{-1} gentamycin (complete RPMI). Hybridomas were selected in complete RPMI supplemented with HAT media and BM-Condimed (Sigma Aldrich).

Cloning, expression and purification of P1 and P1 fragments

The coding sequences for constructs of P1 and the C-terminal domain of P1 were amplified from the synthetic clone of MPN_141 (P1) gene from *M. pneumoniae* (Genscript), using primers P1F and P1R for P1 (29-1521), P1Ct1400_F and P1Ct1400_R for P1 C-terminal (1400-1521), P1Ct1376_F and P1Ct1376_R for P1 C-terminal (1376-1521) (**Supplementary Table 2**). The coding sequences for constructs of P40/P90 were amplified from the synthetic clone of MPN_142 (P40/P90) gene from *M. pneumoniae* (Genscript), using primers P40P90_F and P40P90_R (23-1114) (**Supplementary Table 2**). The PCR fragments were cloned into the expression vector pOPINE (-) to add a C-terminal His-tag to the resulting constructs. Recombinant proteins were obtained after expression with B834

(DE3) cells (Merck), with IPTG at 0.8 mM and 22ºC overnight. The cell pellets were lysed in 1xPBS at pH 7.4 and 40 mM Imidazole (binding buffer) and centrifuged at 20000 RPM at 4ºC. Supernatant was charged into a HisTrap 5ml column (GE Healthcare) and eluted with a buffer containing 400mM imidazole. Soluble aliquots were concentrated and loaded in a Superdex 200 GL 10/300 column (GE Healthcare) with a Tris·HCl 20mM buffer (pH 7.4) and 150mM NaCl.

Production and validation of polyclonal antibodies

Polyclonal antibodies anti-P1, anti-P1 fragments and anti-P90/P40 were obtained by immunizing BALB/C mice with the respective recombinant proteins and polypeptides described above. Polyclonal sera were obtained by cardiac puncture of properly euthanized mice just before splenectomy and tittered using serial dilutions of each antigen. Titers of the different polyclonal sera were determined as the IC_{50} value from four parameter logistic plots and found to be approximately between 1/2500 and 1/4000.

Production and sequencing of the monoclonal antibody P1/MCA4

A *P1* gene fragment was amplified by PCR from genomic DNA of *M. pneumoniae* M129 strain using primers 5'-AGGCCATGGCGGCCTTTCGTGGCAGTTG-3' and 5'-GTGCTCGAGTCATAAATACTAAGCGGGTT-3'. The amplified fragment was inserted into NcoI and XhoI site of pET-30c(+) expression vector, resulting the pP1-8 plasmid (**Supplementary Table 5**). *E. coli* BL21(DE3) was transformed by the pP1-8 for expression of a recombinant P1 peptide containing Ala1160 to Gln1518 of the P1 of M129 strain. The recombinant P1 was purified by His-tag affinity chromatography and used to immunize mice for production of anti-P1 monoclonal antibody. The monoclonal antibody P1/MCA4 was selected by ELISA screening and showed high specificity to P1 in Western blotting analysis and immunofluorescence microscopy of living *M. pneumoniae* cells. The amino acid sequence of P1/MCA4 was determined at GenScript (Tokyo, Japan) by cloning and sequencing of the cDNAs of antibody mRNA from P1/MCA4 producing hybridoma cell. The obtained sequences for a single H chain and two L chain of the P1/MCA4 (**Supplementary Figure 1**) were deposited into the DDBJ/ENA/GenBank databases under the accession numbers LC600310, LC600311 and LC600312.

Purification of the Fab fragment

Monoclonal antibody P1/MCA4 against P1 was diluted up to 2 mg/ml in 1xPBS buffered at pH 8.0 and mixed with 0,1 mg/ml of Papain (previously activated in 20 mM L-cysteine, 20 mM EDTA and 1xPBS pH: 7.0) in a relation 1:40 (Protein:Papain) and incubated during 4 hours at 37ºC. To stop digestion, 10% of the final volume of Iodine acetamide was added. The digested solution was loaded onto HiTrap Protein G 5ml with Binding buffer (20 Mm Na_2HPO_4 pH:7.0) and Elution buffer (0.1 M Glycine·HCl pH 2.7). Soluble aliquots were concentrated and loaded in a Superdex 75 GL 10/300 column (GE Healthcare) with a Tris·HCl 20 mM pH 7.4 and 150 mM NaCl buffer. Complexes of P1-mAb and P1-Fab were formed by mixing both proteins in a ratio 2:1 and 1:1, respectively.

Epitope mapping of Monoclonal antibody P1/MCA4

For epitope mapping of P1/MCA4, a series of plasmids that express recombinant P1 peptides were constructed (**Supplementary Table 5**). These plasmids were generated by partial deletion of the pP1-8 plasmid using specific primer sets (**Supplementary Table 5**) and PrimeSTAR Mutagenesis Basal kit (Takara Bio, Shiga, Japan). Recombinant P1 peptides were produced in *E. coli* BL21(DE3) harboring the plasmids, separated by 10-20% gradient-gel SDS-PAGE, and transferred to nitrocellulose membranes. Recombinant P1 peptides on membranes were reacted with 0.5 µg/ml P1/MCA4. After wash of the membranes, binding of the P1/MCA4 to P1 peptide was detected by anti-mouse IgG, HRP conjugate secondary antibody (Promega, Madison, WI, USA) and EzWestBlue W substrate (Atto, Tokyo, Japan).

Size Exclusion Chromatography and Multi Angle Light Scattering (SEC-MALS)

Molecular weights were measured using a Superdex 200 10/300 GL (GE HEalthcare) column in a Prominence liquid chromatography system (Shimadzu) connected to a DAWN HELEOS II multi-angle light scattering (MALS) detector and an Optilab T-REX refractive index (dRI) detector (Wyatt Technology). ASTRA 7 software (Wyatt Technology) was used for data processing and result analysis. A dn/dc value of 0.185 ml/g (typical of proteins) was assumed for calculations.

Single-particle cryo-EM of the binary complex

To prevent preferred orientation, Octylthioglucoside (OG) was added to solution of purified P1-Fab(P1/MCA4) complex to adjust the final concentration of OG to 0.9% (w/l). 2.6 µL of sample solution was applied to a glow-discharged Au-coated Quantifoil holey carbon grid (R1.2/1.3, Cu, 200 mech), blotted for 4 sec at 4°C in 100% humidity and plunged into frozen liquid ethane using a Vitrobot Mark IV (Thermo Fisher Scientific). The grid was inserted into a CRYO ARM 300 (JEOL) operating at an acceleration voltage of 300 kV. CryoEM images were recorded with a K3 direct electron detector (Gatan) in CDS mode with an energy filter at a slit width of 20 eV. Data were automatically collected using the SerialEM software (https://bio3d.colorado.edu/SerialEM/) at a physical pixel size of 0.49 Å with 50 frames at a dose of 2.0 e^{-}/ Å ^{2} per frame and an exposure time of 2.86 sec per movie with a defocus ranging from -0.5 to -1.5 µm. A total of 27,122 movies were collected for P1-Fab complex. The movie frames were subjected to beam-induced movement correction using MotionCor2.1(Zheng et al., 2017) and contrast transfer function (CTF) was evaluated using Gctf (Zhang, 2016). Approximately 2,000 particles were manually selected from 20 micrographs to perform two-dimensional (2D) classification. Using a good 2D class average image, a total of 4,312,408 particle images were automatically picked and 2D classifications were performed using RELION-3.1 (Zivanov et al., 2018). A total of 1,252,491 particles were selected for building the initial model of the P1-Fab complex using cryoSPARC2 (Punjani et al., 2017) and subjected to 3D classification into 8 classes using RELION-3.1. The selected particles were re-extracted at a pixel size of 0.49 Å and subjected to three 3D refinement, two CTF refinement and Bayesian polishing. After selection of particles using no-alignment 3D classification, a total of 352,039 particles were subjected to two 3D refinement and CTF refinement. The final 3D refinement and post-processing yielded maps with global resolutions of 2.39 Å, according to the 0.143 criterion of the Fourier shell correlation. Local resolution was estimated using RELION-3.1. The processing strategy is described in **Supplementary Fig 4**

(Supplementary Table IA).

Model building and refinement of the binary complex

The model of the P1-Fab complex was built based on the cryoEM density map. Previous published crystal structure of P1 (PDB ID: 6RC9) was docked into the EM density map using UCSF Chimera (Punjani et al., 2017). N-domain, C-domain of P1 and Fab were manually repositioned and refined iteratively using COOT (Emsley and Cowtan, 2004) and PHENIX real space refinement (Afonine et al., 2018). The statics of the 3D reconstruction and model refinement are summarized in Table Supplementary Table I B. The final refined structure has been deposited in the EMDB with code XXXX

Single-particle cryo-EM of the ternary complex

2.6 µL of sample solution was applied to a glow-discharged Quantifoil holey carbon grid (R1.2/1.3, Cu, 200 mech), blotted for 4 sec at 4°C in 100% humidity and plunged into frozen liquid ethane using a Vitrobot Mark IV. The grid was inserted into a CRYO ARM 300 operating at an acceleration voltage of 300 kV. CryoEM images were recorded with a K3 direct electron detector in CDS mode with an energy filter at a slit width of 20 eV. Data were automatically collected using the SerialEM software (https://bio3d.colorado.edu/SerialEM/) at a physical pixel size of 0.87 Å with 40 frames at a dose of 2.0 e^{-}/ Å ^{2} per frame and an exposure time of 3.3 sec per movie with a defocus ranging from -0.8 to -1.8 µm. A total of 7,938 movies were collected for P40/P90-P1-Fab complex.

The movie frames were subjected to beam-induced movement correction using MotionCor2.1 and CTF was evaluated using Gctf. Using blob picker program of cryoSPARC2, a total of 9,565,198 particle images were automatically picked and 2D classifications were performed using cryoSPARC2. A total of 1,070,120 particles were selected for building the initial model of the P40/P90-P1-Fab complex using cryoSPARC2. However, due to preferred orientation, an accurate initial structure could not be obtained. Therefore, we did not perform 3D reconstruction for high-resolution structure determination, but performed 3D refinement to confirm how P40/P90 and Fab are bound to P1. The selected particles were re-extracted at a pixel size of 0.87 Å and subjected to 3D refinement. The final 3D refinement and post-processing yielded maps with global resolutions of below 10 Å, according to the 0.143 criterion of the Fourier shell correlation **(Supplementary Table 2)**.

DNA manipulation and primers.

Plasmid DNA was purified using GeneJET Plasmid Miniprep Kit (Thermo Fisher Scientific). PCR products and DNA fragments were recovered from agarose gels using NucleoSpin Gel and PCR Clean-up Kit (Macherey-Nagel, Düren, Germany), and digested using the corresponding restriction enzymes (Thermo Fisher Scientific) when necessary. For transformation of *M. genitalium*, plasmids were purified using the GenElute HP Midiprep Kit (Sigma-Aldrich, St. Louis, USA) following the manufacturer's instructions. All primers used in this study are listed in **Supplementary Table X**.

***Plasmid construction and mutant obtention.* (G37ΔAdh and complemented Engelman mutant strains)**

The suicide plasmid pBEΔMG_191/MG_192 was designed to generate a G37 M. genitalium MG_191 and MG_192 null mutant strain by gene replacement. First, a 1 kb flanking upstream region (UR) to the MG_191 gene was PCR-amplified using the MgParUp-F and MgParUp-R primers. Similarly, a 1 kb flanking downstream region to the MG_192 gene was PCR-amplified with the MgParDw-F and MgParDw-R primers. In parallel, the a lox version of the CmM438 selectable marker (Torres-Puig et al., 2015) was PCR-amplified with the Lox71p438-Fwd-XhoI and CatLox66-Rev-BamHI primers, obtaining the CmM438 flanked with the lox61 and lox71 sequences. Then, the UR and DR PCR products were joined by PCR with the MgParUp-F and MgParDw-R primers. The resulting PCR product was cloned into an EcoRV-digested pBE plasmid (Pich et al., 2006). Finally, the resulting CmM438 amplicon was digested with XhoI and BamHI restriction enzymes and ligated into the similarly digested pBE containing the UR and DR regions obtained before.

This plasmid was used to obtain the G37ΔAdh chloramphenicol resistant mutant strain. Electroporation of this mutant with the pCre plasmid (Mariscal et al., 2016) that contains the Cre recombinase allowed us to obtain the G37ΔAdh strain, free of any antibiotic selectable marker. This strain was used as the recipient strain to transform all the pMTnPac plasmids generated in this study.

MG_191 and MG_192 genes from the chromosome of M. genitalium G37 strain were amplified by PCR using COMmg191-F-ApaI and COMmg191/192-R-SalI primers. The resulting PCR product was cloned into an EcoRV-digested pBE plasmid to create the pBE-COMP140P110. At the same time, the amplicon was digested with the ApaI and SalI

563 restriction enzymes and ligated to a similarly digested pMTnPac plasmid to create the
564 pTnPacCOMP140P110. This plasmid was used to reintroduce the wild-type alleles of the
565 MG_191 and MG_192 genes to the G37ΔAdh mutant. The COMmg192-F (ApaI) primer
566 includes the upstream region (70 nucleotides) of the MG_191 gene, which contains a strong
567 promoter identified in a previous study (Musatovova et al., 2003). This promoter was used
568 to drive the transcription of the transposon-encoded copy of the MG_191 and MG_192 genes
569 in all mutants.

570 To generate P140 and P110 variants carrying specific mutations in the Engelman
571 motifs, the target mutations in the MG_191 and or MG_192 genes were introduced by Exsite-
572 PCR using the pBE-COMP140P110 as a template and the specific primers for each mutant
573 (Supplementary Table X.). Then, plasmids containing the P140 and P110 alleles with the
574 desired mutations were re-ligated and mutant P140 and P110 alleles excised by digestion
575 with ApaI and SalI restriction enzymes. Finally, DNA fragments with mutant alleles were
576 ligated into a pMTnPac plasmid previously digested with ApaI and SalI, to generate the
577 corresponding pMTnPacCOMP140P110 plasmid series.

578 Sequencing analysis of the different TnPacCOMP140P110 constructs using primers
579 Tnp3, RTPCR192-F, RTPCR192-R, and PacUp, ruled out the presence of additional
580 mutations in the MG_191 and MG_192 sequences. These plasmids were transformed into
581 the *M. genitalium* G37ΔAdh null mutant to create the different P140 and P110 variant strains.
582 Identification of the minitransposon insertion site in the individual clones was done by
583 sequencing using the PacDown primer and chromosomal DNA as a template.

584

585 ***Transformation and screening.***

586 *M. genitalium* G37ΔAdh null mutants were transformed by electroporation using 10
587 μg of plasmid DNA of the different minitransposons or 30 μg when using plasmids for gene
588 replacement experiments, as previously described (Pich et al., 2006; Torres-Puig et al., 2018).
589 Puromycin-resistant colonies were picked, propagated, and stored at –80 °C. For screening
590 purposes, strains were further propagated in antibiotic supplemented SP4 medium in 25 cm^2
591 tissue culture flasks. To obtain crude lysates from grown cultures, SP4 medium was removed
592 and cells were lysed using 50 μl of Lysis Buffer (0.1M Tris-HCl pH 8.5, 0.05% Tween-20,
593 and 250 μg ml^{-1} Proteinase K) and incubated for 1 h at 37 °C. Then, Proteinase K was

inactivated at 96 °C for 10 min. *M. genitalium* lysates were screened by PCR or direct Sanger sequencing using the primers in Supplementary table X

Sequencing reactions.

DNA sequencing reactions were performed using BigDye® v3.1 Cycle Sequencing kit using 2.5µl of genomic DNA or *M. genitalium* lysate, following manufacturer's instructions (Thermo Fisher Scientific). All reactions were analysed in an ABI PRISM 3130xl Genetic Analyzer at the Servei de Genòmica i Bioinformàtica (UAB).

SDS-PAGE and WB.

Whole-cell lysates were obtained from mid-log phase cultures grown in 75 cm^2 flasks. Protein concentration was determined with the Pierce™ BCA Protein Assay Kit (Thermo Fisher Scientific), and similar amounts of total protein were separated by SDS-PAGE following the standard procedures.

For specific detection of M. genitalium proteins, SDS-PAGE gels were electrotransferred to PVDF membranes by a Semi-dry transfer System, using cold Towbin buffer (25mM Tris, 192mM Glycine pH 8.3-8.4, 20% Methanol (v/v)) following the standard protocols (Mahmood and Yang, 2012; Towbin et al., 1979). Membranes were probed with the appropriate primary antibody in blocking solution, which was then detected using a secondary antibody conjugated with horseradish peroxidase (Bio-Rad). Antibodies used in this study are listed in the **Supplementary Table 6.** Bioluminescence reaction was catalyzed with *Luminata Forte™ Western HRP substrate* (Merk Millipore). Visualization and image optimization was performed in a VersaDoc Imaging System (Bio-Rad) using QuantityOne® software (Bio-Rad).

Quantitative hemadsorption assay.

Hemadsorption was quantified using flow cytometry as previously described (García-Morales et al., 2014) with few modifications. We used 10^9 mycoplasma cells for the hemadsorption assay. Fluorescence-activated cell sorting (FACS) data were acquired using a FACSCalibur (Becton Dickinson, Franklin Lakes, USA) equipped with an air-cooled 488 nm argon laser and a 633 nm red diode laser and analysed with the CellQuest-Pro and

FACSDiva software (Becton Dickinson). Binding of mycoplasma cells to red blood cells was modelled in an inverse Langmuir isothermal kinetic function:

$$M_f = 1 - \frac{B_{max}[RBC]}{K_d + [RBC]}$$

The plots represent the best-fitting curves to a series of hemadsorption measurements obtained from at least two biological repeats for each strain. We performed a double-gating strategy, using a preliminary FL3-H/FL2-H gate following an SSC-H/FL1-H gate.

Time lapse micro-cinematography

Effects of antibody sera on mycoplasma cells were investigated by time lapse cinematography of *M. pneumoniae* cells growing in IBIDI 8-well chamber slides. Prior to observation the medium was replaced with PBS containing 10% Fetal Bovine Serum and 3% gelatin pre-warmed at 37°C. After incubation for 10 minutes at 37 ºC and 5% CO_2, the slide was placed in a Nikon Eclipse TE 2000-E inverted microscope equipped with a Microscope Cage Incubation System (Okolab) at 37 ºC. Images were captured at 0.5 s intervals for a total observation time of 10 min, and the different antibodies were dispensed directly into the wells after the first 50 seconds of observation. Frequencies of motile cells and detached cells before adding the different antibodies were calculated from the images collected between 0 and 50 seconds of observation. Frequencies of motile cells and detached cells after adding the different antibodies were calculated from the pictures collected between 50 seconds and 10 minutes of observation.

Immunofluorescence microscopy

The immunofluorescence staining of mycoplasma cells on chamber slides was similar to previously described (Nakane et al., 2015; Sprankel et al., 2023), with several modifications. All mycoplasma cells were washed with PBS containing 0.02% Tween 20 (PBS-T) except cells from *M. genitalium* G37ΔAdh strain and Engelman motif mutant strains, which were washed in PBS containing 136 mM sucrose (PBS-Suc), prewarmed at 37 °C. Then, each well was fixed with 200 µL of 3% paraformaldehyde (wt/vol) and 0.1% glutaraldehyde. Cells were washed three times with PBS-T (or PBS-Suc), and slides were immediately treated with 3% BSA in PBS-T (blocking solution) for 30 minutes. The blocking

solution was removed and each well was incubated for 1 hour with 200 μL of the primary antibodies diluted in blocking solution. We have used a 1/2000 dilution for all polyclonal sera. Wells were washed three times with PBS-T or PBS-Suc and incubated for 1 hour with a 1/2,000 dilution of a goat anti-mouse Alexa 555 secondary antibody (Invitrogen) in blocking solution. Wells were then washed three times with PBS-T or PBS-Suc and incubated for 20 minutes with 100 μL of a solution of Hoechst 33342 10 μg/μL in PBS-T or PBS-Suc. Wells were finally washed once with PBS-T and replenished with 200 μL of PBS-T. Cells were examined by phase contrast and epifluorescence in an Eclipse TE 2000-E inverted microscope (Nikon). Phase contrast images, 4',6-diamidino-2-phenylindole (DAPI, excitation 387/11 nm, emission 447/60 nm) and Texas Red (excitation 560/20 nm, emission 593/40 nm) epifluorescence images were captured with an Orca Fusion camera (Hamamatsu) controlled by NIS-Elements BR software (Nikon).

Acknowledgements

We are most thankful to Dr. X. Daura for his help in the epitope prediction study. We also thank L. Company and I. Fernández-Vidal for their support during MALS measurements, and to A. Iborra (Servei de Cultius Cellulars, Anticossos Citometria, UAB) for his assistance with immunizing mice. J. P. and I. F. were funded by Ministerio de Ciencia, Innovación y Universidades (MICINN, Spain) with grants PID2021-125632OB-C22 and -C21, respectively.

References

Afonine, P.V., Poon, B.K., Read, R.J., Sobolev, O.V., Terwilliger, T.C., Urzhumtsev, A., Adams, P.D., 2018. Real-space refinement in PHENIX for cryo-EM and crystallography. Acta Crystallogr D Struct Biol 74, 531–544. https://doi.org/10.1107/S2059798318006551

Aparicio, D., Scheffer, M.P., Marcos-Silva, M., Vizarraga, D., Sprankel, L., Ratera, M., Weber, M.S., Seybert, A., Torres-Puig, S., Gonzalez-Gonzalez, L., Reitz, J., Querol, E., Piñol, J., Pich, O.Q., Fita, I., Frangakis, A.S., 2020. Structure and mechanism of the Nap adhesion complex from the human pathogen Mycoplasma genitalium. Nature communications 11. https://doi.org/10.1038/S41467-020-16511-2

Aparicio, D., Torres-Puig, S., Ratera, M., Querol, E., Piñol, J., Pich, O.Q., Fita, I., 2018. Mycoplasma genitalium adhesin P110 binds sialic-acid human receptors. Nature Communications 9. https://doi.org/10.1038/s41467-018-06963-y

Burgos, R., Pich, O.Q., Ferrer-Navarro, M., Baseman, J.B., Querol, E., Piñol, J., 2006. Mycoplasma genitalium P140 and P110 cytadhesins are reciprocally stabilized and required for cell adhesion and terminal-organelle development. J Bacteriol 188, 8627–8637. https://doi.org/10.1128/JB.00978-06

Emsley, P., Cowtan, K., 2004. Coot: model-building tools for molecular graphics. Acta Crystallogr D Biol Crystallogr 60, 2126–2132. https://doi.org/10.1107/S0907444904019158

García-Morales, L., González-González, L., Costa, M., Querol, E., Piñol, J., 2014. Quantitative assessment of Mycoplasma hemadsorption activity by flow cytometry. PloS one 9. https://doi.org/10.1371/JOURNAL.PONE.0087500

Henderson, G.P., Jensen, G.J., 2006. Three-dimensional structure of Mycoplasma pneumoniae's attachment organelle and a model for its role in gliding motility. Molecular Microbiology 60. https://doi.org/10.1111/j.1365-2958.2006.05113.x

Kasai, T., Nakane, D., Ishida, H., Ando, H., Kiso, M., Miyata, M., 2013. Role of binding in Mycoplasma mobile and Mycoplasma pneumoniae gliding analyzed through inhibition by synthesized sialylated compounds. Journal of bacteriology 195, 429–435. https://doi.org/10.1128/JB.01141-12

Kawamoto, A., Matsuo, L., Kato, T., Yamamoto, H., Namba, K., Miyata, M., 2016. Periodicity in Attachment Organelle Revealed by Electron Cryotomography Suggests Conformational Changes in Gliding Mechanism of Mycoplasma pneumoniae. mBio 7. https://doi.org/10.1128/MBIO.00243-16

Köhler, G., Milstein, C., 2005. Continuous cultures of fused cells secreting antibody of predefined specificity. 1975. J Immunol 174, 2453–2455.

Krause, D.C., Leith, D.K., Wilson, R.M., Baseman, J.B., 1982. Identification of Mycoplasma pneumoniae proteins associated with hemadsorption and virulence. Infection and Immunity 35. https://doi.org/10.1128/iai.35.3.809-817.1982

Mahmood, T., Yang, P.C., 2012. Western blot: technique, theory, and trouble shooting. North American journal of medical sciences 4, 429–434. https://doi.org/10.4103/1947-2714.100998

Mariscal, A.M., González-González, L., Querol, E., Piñol, J., 2016. All-in-one construct for genome engineering using Cre-lox technology. DNA Research 23. https://doi.org/10.1093/dnares/dsw015

Mazzolini, R., Rodríguez-Arce, I., Fernández-Barat, L., Piñero-Lambea, C., Garrido, V., Rebollada-Merino, A., Motos, A., Torres, A., Grilló, M.J., Serrano, L., Lluch-Senar, M., 2023. Engineered live bacteria suppress Pseudomonas aeruginosa infection in mouse lung and dissolve endotracheal-tube biofilms. Nature biotechnology. https://doi.org/10.1038/S41587-022-01584-9

Miyata, M., 2008. Centipede and inchworm models to explain Mycoplasma gliding. Trends in microbiology 16, 6–12. https://doi.org/10.1016/J.TIM.2007.11.002

Miyata, M., Hamaguchi, T., 2016. Integrated Information and Prospects for Gliding Mechanism of the Pathogenic Bacterium Mycoplasma pneumoniae. Frontiers in microbiology 7. https://doi.org/10.3389/FMICB.2016.00960

Mizutani, M., Miyata, M., 2019. Behaviors and Energy Source of Mycoplasma gallisepticum Gliding. Journal of bacteriology 201. https://doi.org/10.1128/JB.00397-19

Mizutani, M., Sasajima, Y., Miyata, M., 2021. Force and Stepwise Movements of Gliding Motility in Human Pathogenic Bacterium Mycoplasma pneumoniae. Frontiers in Microbiology 12. https://doi.org/10.3389/fmicb.2021.747905

Musatovova, O., Dhandayuthapani, S., Baseman, J.B., 2003. Transcriptional starts for cytadherence-related operons of Mycoplasma genitalium. FEMS Microbiology Letters 229. https://doi.org/10.1016/S0378-1097(03)00789-4

Nakane, D., Kenri, T., Matsuo, L., Miyata, M., 2015. Systematic Structural Analyses of Attachment Organelle in Mycoplasma pneumoniae. PLoS Pathogens 11. https://doi.org/10.1371/journal.ppat.1005299

Parrott, G.L., Kinjo, T., Fujita, J., 2016. A Compendium for Mycoplasma pneumoniae. Frontiers in microbiology 7. https://doi.org/10.3389/FMICB.2016.00513

Pich, O.Q., Burgos, R., Planell, R., Querol, E., Piñol, J., 2006. Comparative analysis of antibiotic resistance gene markers in Mycoplasma genitalium: application to studies of the minimal gene complement. Microbiology (Reading, England) 152, 519–527. https://doi.org/10.1099/MIC.0.28287-0

Pich, O.Q., Burgos, R., Querol, E., Piñol, J., 2009. P110 and P140 cytadherence-related proteins are negative effectors of terminal organelle duplication in Mycoplasma genitalium. PLoS One 4, e7452. https://doi.org/10.1371/journal.pone.0007452

Punjani, A., Rubinstein, J.L., Fleet, D.J., Brubaker, M.A., 2017. cryoSPARC: algorithms for rapid unsupervised cryo-EM structure determination. Nat Methods 14, 290–296. https://doi.org/10.1038/nmeth.4169

Rangroo, R., Young, M., Davis, A., Pack, S., Thakore, S., Schepcoff, A., Oyesanmi, O., 2022. The Severity of the Co-infection of Mycoplasma pneumoniae in COVID-19 Patients. Cureus 14. https://doi.org/10.7759/CUREUS.24563

Scheffer, M.P., Gonzalez-Gonzalez, L., Seybert, A., Ratera, M., Kunz, M., Valpuesta, J.M., Fita, I., Querol, E., Piñol, J., Martín-Benito, J., Frangakis, A.S., 2017. Structural characterization of the NAP; the major adhesion complex of the human pathogen Mycoplasma genitalium. Molecular Microbiology 105. https://doi.org/10.1111/mmi.13743

Seto, S., Kenri, T., Tomiyama, T., Miyata, M., 2005. Involvement of P1 adhesin in gliding motility of Mycoplasma pneumoniae as revealed by the inhibitory effects of antibody under optimized gliding conditions. Journal of Bacteriology 187. https://doi.org/10.1128/JB.187.5.1875-1877.2005

Seybert, A., Gonzalez-Gonzalez, L., Scheffer, M.P., Lluch-Senar, M., Mariscal, A.M., Querol, E., Matthaeus, F., Piñol, J., Frangakis, A.S., 2018. Cryo-electron tomography analyses of terminal organelle mutants suggest the motility mechanism of Mycoplasma genitalium. Mol Microbiol 108, 319–329. https://doi.org/10.1111/mmi.13938

Seybert, A., Herrmann, R., Frangakis, A.S., 2006. Structural analysis of Mycoplasma pneumoniae by cryo-electron tomography. Journal of Structural Biology 156. https://doi.org/10.1016/j.jsb.2006.04.010

Sprankel, L., Vizarraga, D., Martín, J., Manger, S., Meier-Credo, J., Marcos, M., Julve, J., Rotllan, N., Scheffer, M.P., Escolà-Gil, J.C., Langer, J.D., Piñol, J., Fita, I., Frangakis, A.S., 2023. Essential protein P116 extracts cholesterol and other indispensable lipids for Mycoplasmas. Nature Structural and Molecular Biology 30. https://doi.org/10.1038/s41594-023-00922-y

Torres-Puig, S., Broto, A., Querol, E., Piñol, J., Pich, O.Q., 2015. A novel sigma factor reveals a unique regulon controlling cell-specific recombination in Mycoplasma genitalium. Nucleic acids research 43, 4923–4936. https://doi.org/10.1093/NAR/GKV422

Torres-Puig, S., Martínez-Torró, C., Granero-Moya, I., Querol, E., Piñol, J., Pich, O.Q., 2018. Activation of σ20-dependent recombination and horizontal gene transfer in Mycoplasma genitalium. DNA Res 25, 383–393. https://doi.org/10.1093/dnares/dsy011

Towbin, H., Staehelin, T., Gordon, J., 1979. Electrophoretic transfer of proteins from polyacrylamide gels to nitrocellulose sheets: procedure and some applications. Proceedings of the National Academy of Sciences of the United States of America 76, 4350–4354. https://doi.org/10.1073/PNAS.76.9.4350

Vizarraga, D., Kawamoto, A., Matsumoto, U., Illanes, R., Pérez-Luque, R., Martín, J., Mazzolini, R., Bierge, P., Pich, O.Q., Espasa, M., Sanfeliu, I., Esperalba, J., Fernández-Huerta, M., Scheffer, M.P., Pinyol, J., Frangakis, A.S., Lluch-Senar, M., Mori, S., Shibayama, K., Kenri, T., Kato, T., Namba, K., Fita, I., Miyata, M., Aparicio, D., 2020. Immunodominant proteins P1 and P40/P90 from human pathogen Mycoplasma pneumoniae. Nature Communications 11. https://doi.org/10.1038/s41467-020-18777-y

Vizarraga, D., Torres-Puig, S., Aparicio, D., Pich, O.Q., 2021. The Sialoglycan Binding Adhesins of Mycoplasma genitalium and Mycoplasma pneumoniae. Trends in microbiology 29, 477–481. https://doi.org/10.1016/J.TIM.2021.01.011

Waites, K.B., Xiao, L., Liu, Y., Balish, M.F., Atkinson, T.P., 2017. Mycoplasma pneumoniae from the Respiratory Tract and Beyond. Clinical Microbiology Reviews 30, 747. https://doi.org/10.1128/CMR.00114-16

Williams, C.R., Chen, L., Sheppard, E.S., Chopra, P., Locklin, J., Boons, G.J., Krause, D.C., 2020. Distinct mycoplasma pneumoniae interactions with sulfated and sialylated receptors. Infection and Immunity 88. https://doi.org/10.1128/IAI.00392-20

Zhang, K., 2016. Gctf: Real-time CTF determination and correction. J Struct Biol 193, 1–12. https://doi.org/10.1016/j.jsb.2015.11.003

Zheng, S.Q., Palovcak, E., Armache, J.-P., Verba, K.A., Cheng, Y., Agard, D.A., 2017. MotionCor2: anisotropic correction of beam-induced motion for improved cryo-electron microscopy. Nat Methods 14, 331–332. https://doi.org/10.1038/nmeth.4193

Zivanov, J., Nakane, T., Forsberg, B.O., Kimanius, D., Hagen, W.J., Lindahl, E., Scheres, S.H., 2018. New tools for automated high-resolution cryo-EM structure determination in RELION-3. Elife 7, e42166. https://doi.org/10.7554/eLife.42166

Figure 1

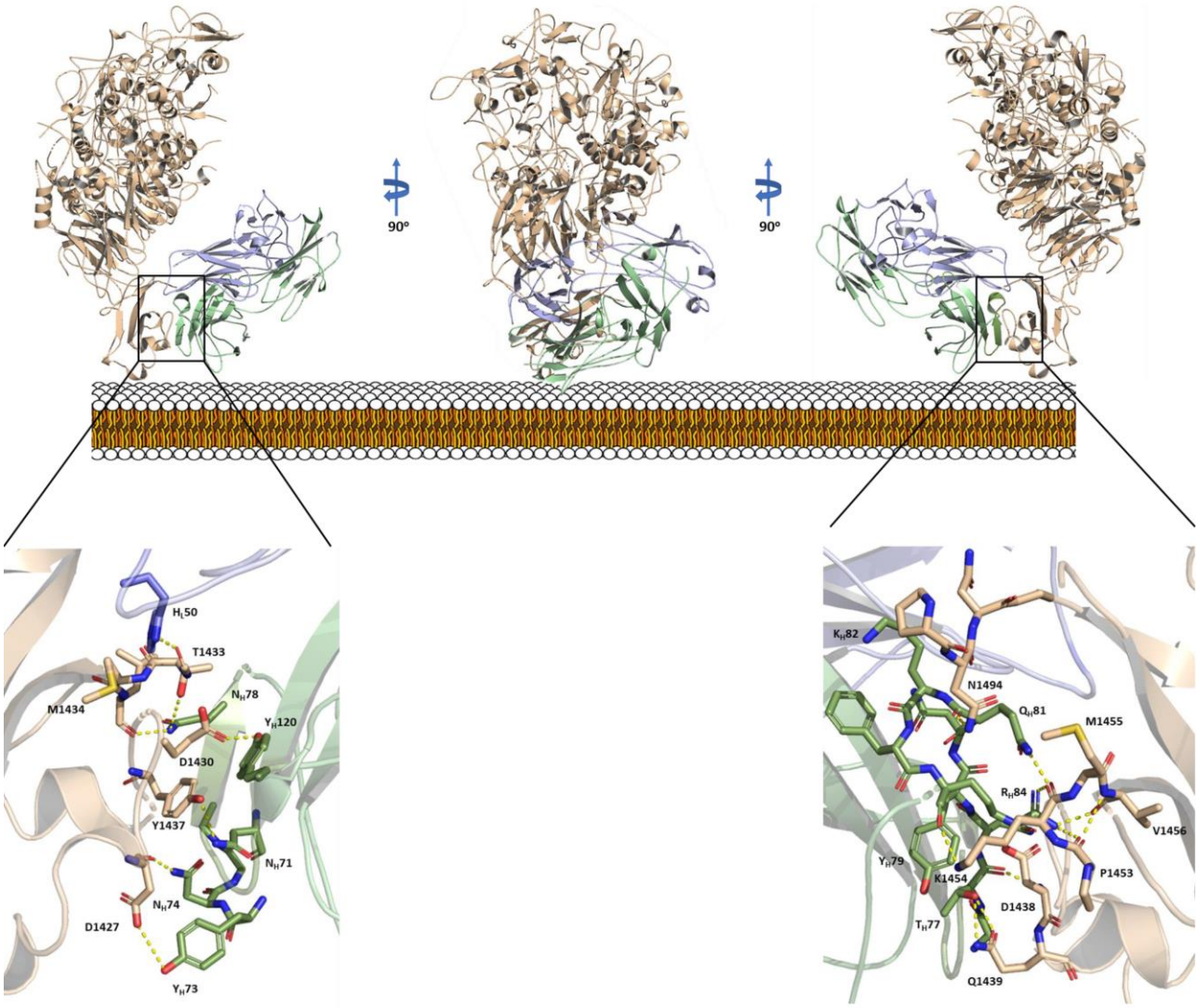
90°
90°
H_L50
T1433
M1434
N_H78
Y_H120
D1430
Y1437
N_H71
N_H74
D1427
Y_H73
K_H82
N1494
Q_H81
M1455
R_H84
V1456
Y_H79
K1454
P1453
D1438
T_H77
Q1439

Figure 2

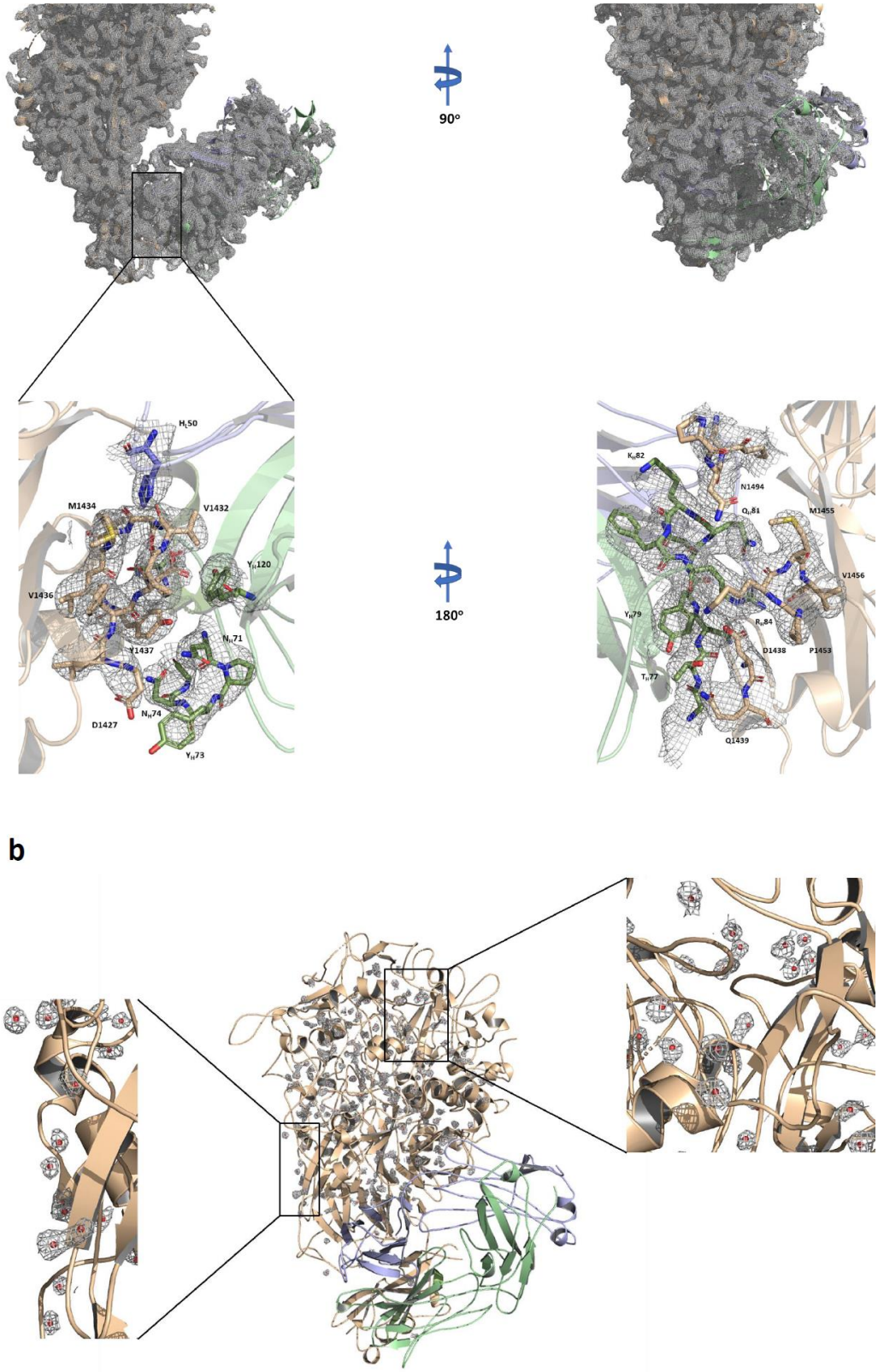
90°
180°
M1434
V1432
V1436
V1437
D1427
N1494
M1455
V1456
P1453
D1438
Q1439
b

825

Figure 3

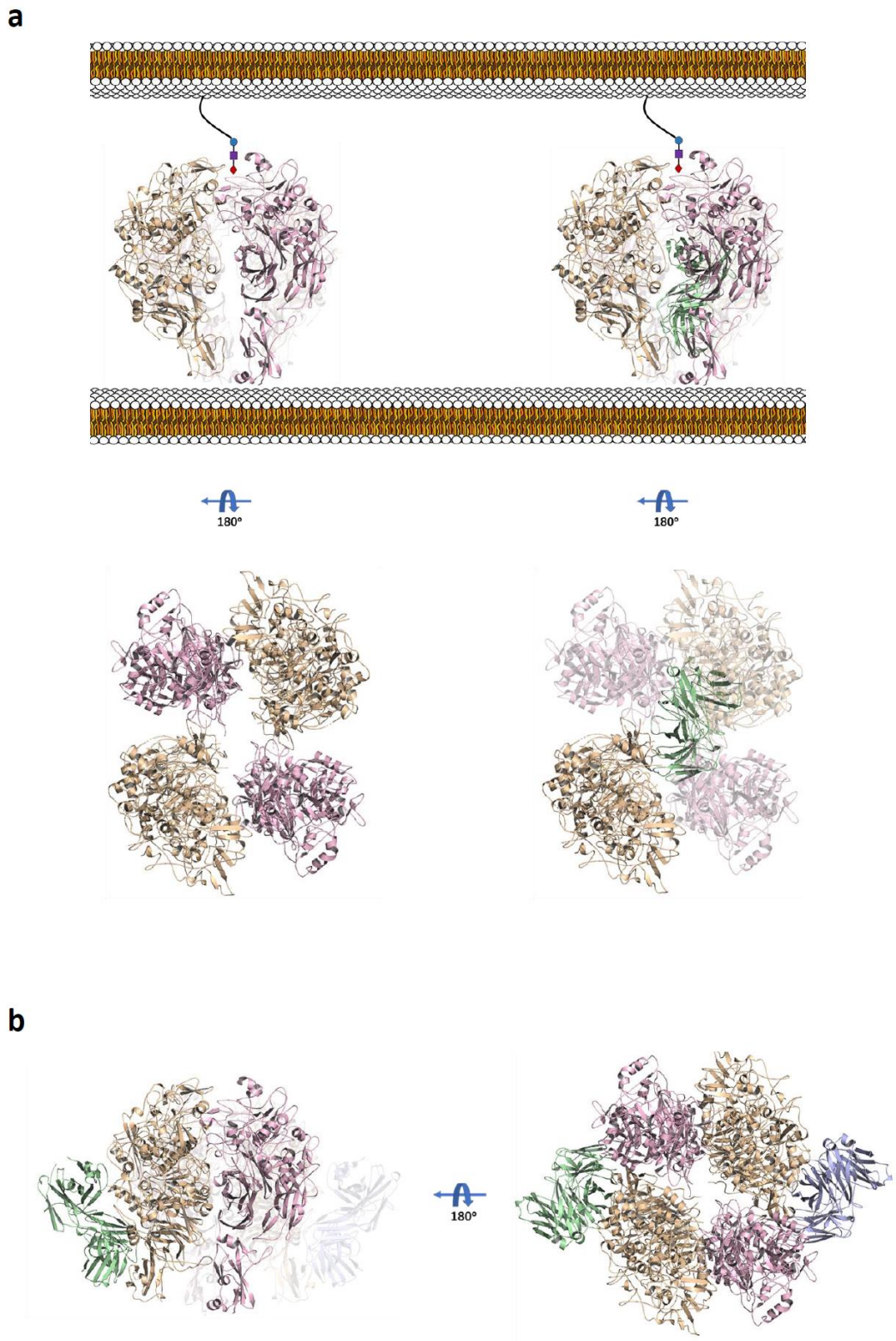

826

Figure 4

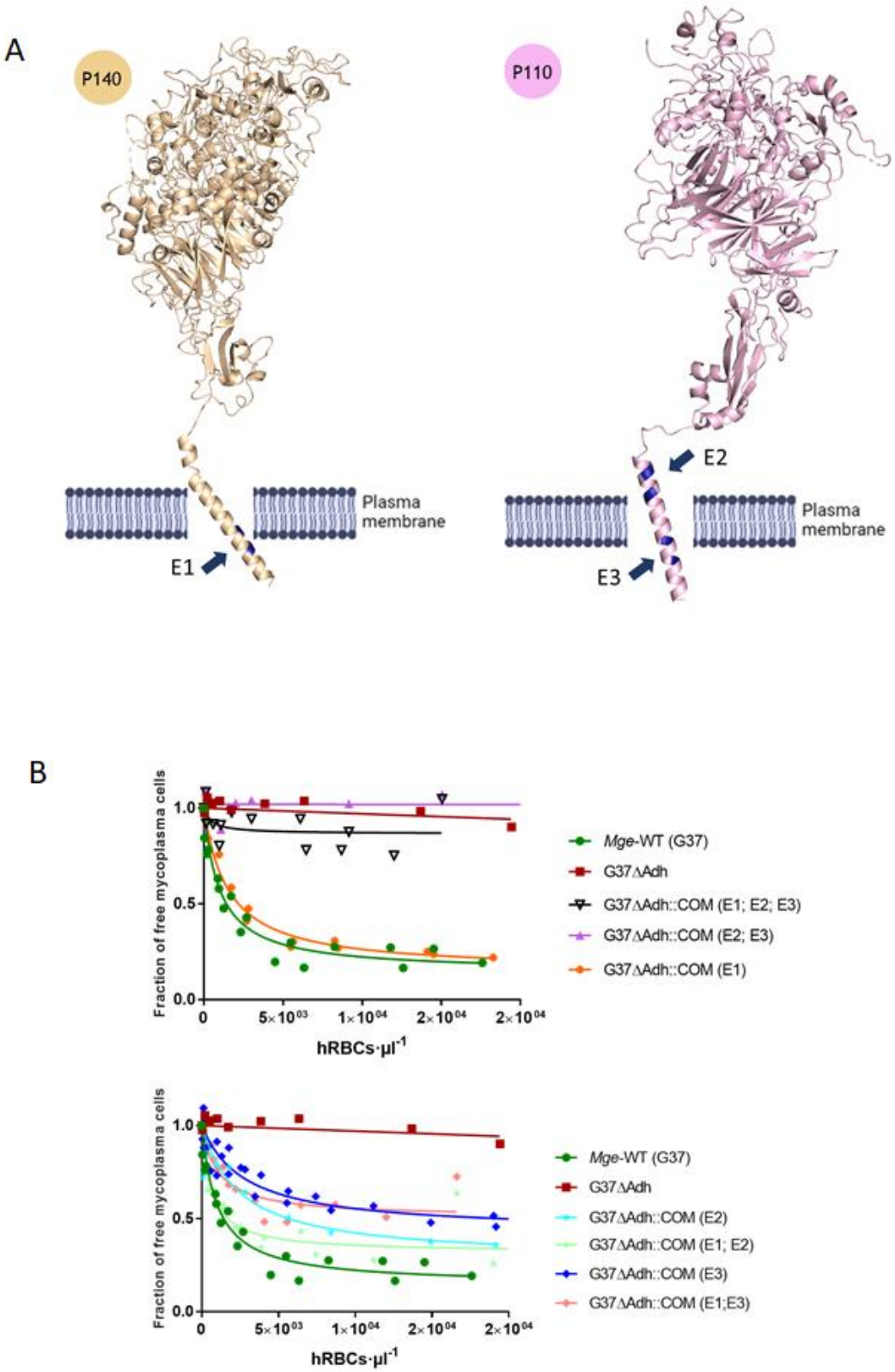

827

Figure 5

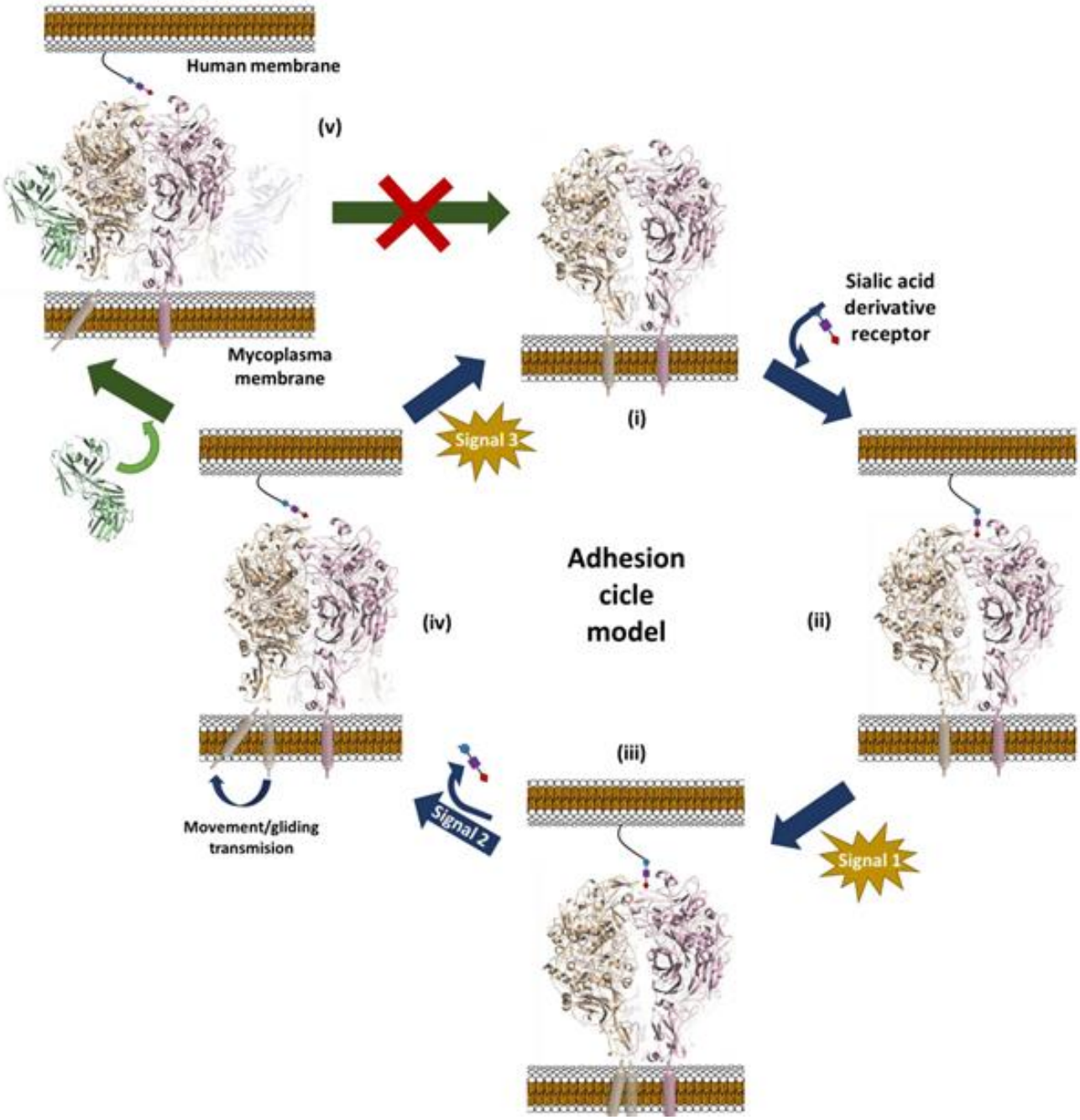
Human membrane
(v)
Mycoplasma membrane
Sialic acid derivative receptor
(i)
Signal 3
Adhesion cicle model
(ii)
(iv)
(iii)
Movement/gliding transmision
Signal 2
Signal 1

Figure Captions

Figure 1. **Cryo-EM structure of the P1-Fab(P1/MCA4) complex**

Ribbon representations, with three 90° apart views, of the complex between P1 (brown) and the Fab fragment of the monoclonal antibody P1/MCA4 (light and heavy chains in blue and green, respectively). Insets show 180° apart views of the recognition interactions between P1 and P1/MCA4. The epitope is located in the C-terminal domain of P1, close to the mycoplasma membrane (displayed as a reference).

Figure 2. Cryo-EM map of the P1-Fab(P1/MCA4) complex

Two 90° apart views of the whole cryo-EM map of the P1-Fab(P1/MCA4) complex. The map is crispy, with well-defined side chains, for most of P1 and also for the Fab variable module (V_L-V_H). The insets show two 180° apart views of the map at the epitope-paratope interface (same color code as in Figure 1).

Figure 3. The Nap in complex with Fab (P1/MCA4)

A) "Open" conformation of the Nap with one of the P1 subunits replaced by the P1-Fab(P1/MCA4) complex results in the brutal steric clash of the Fab with the Nap. The epitope, buried in the Nap center, is total inaccessibility to antibodies. In the "open" conformation the Nap can attach to sialylated receptors and two membranes, corresponding to the mycoplasma and to the cell host (lower and upper membranes, respectively), are displayed as a reference. B) "Closed" conformation of the Nap with P1 subunits replaced by P1-Fab(P1/MCA4) complexes where C-terminal domains have rotated avoiding steric clashes.

Figure 4. Engelman motifs in adhesines

A) Transmembrane helices from adhesins contain highly conserved Engelman motifs. B) Mutational analysis, performed in the adhesins P140 and P110 from *M. genitalium*, indicate that Engelman motifs from P110 have a significant contribution to motility. On the contrary, no effects were observed when the Engelman motif from P140 was mutated.

Figure 5. The Nap attachment and detachment cycle

Naps involved in gliding have to cycle between "open" and "closed" conformations, with the binding site for the sialylated receptors becoming alternatively accessible and inaccessible. During the cycle, the C-terminal domain of P1 experiences important rearrangements changing the exposed surfaces. Monoclonal antibody P1/MCA4 traps the "closed" conformation halting the Nap cycle and interfering with binding.

Supplementary Figures

Supplementary Figure 1. Mab P1/MCA4 sequence: a) Heavy and b) Light chains.

Supplementary Figure 2. MALS from the C-terminal domain of P1 a) Mab P1/MCA4 and b) Fab P1/MCA4

Supplementary Figure 3. Epitope mapping (Tsuyoshi)

Supplementary Figure 4. Cryo-EM structure determination of the P1-Fab(P1/MCA4) complex (Aki-Keiichi)

Supplementary Figure 5. Map quality of the P1-Fab(P1/MCA4) complex: Identification of solvent molecules

The quality of the map allowed the identification of a large number of solvent molecules in the N-terminal domain of P1.

Supplementary Figure 6. Superposition of P1 structures (from the complex with the Fab and from X-ray)

Supplementary Figure 7. CMALS analysis of binary and ternary complexes of adhesines P1, P40/P90 and Fab(P1/MCA4).

Supplementary Figure 8. Cryo-EM structure determination of the ternary P40/P90-P1-Fab(P1/MCA4) complex (Aki-Keiichi)

Supplementary Figure 9. Partial model of the Ternary complex

Supplementary Figure 10. MALS P140: a) C-domain alignment and b) Several measures. Outcome is no complex, in spite of only small differences

Supplementary Figure 9-10. Nap closed conformation with /without Fab

Supplementary Figure 10-11. C-domain movements…..

Supplementary Tables

Supplementary Table I. Monoclonal antibodies generated against the P1:1160-1518 peptide

Supplementary Table II. Cryo-EM data collection and model refinement statistics of the P1-Fab(P1/MCA4) complex

Supplementary Table III. Cryo-EM data collection and model refinement statistics of the ternary complex

Supplementary Table IV. Inhibitory assays with polyclonal antibodies

Motility status and RT_{50} (time of the MCN by which the half of the cells have stopped) of stopped cells in microcinematography (MCN) replicates of *M. pneumoniae* cells before and after adding polyclonal antibodies (PCA) vs P1 and P40/P90 or monoclonal antibody (MCA4) vs P1. A negative control was performed by incubating cells in the same medium (PBS - 10% FBS) but no antibodies were added. Mean and standard deviation (SD) were computed from the frequencies of motile cells and RT_{50} in each replicate.

Supplementary Table V. Plasmids used for expression of P1 protein franments

Videos

Video I. Effects on *M. pneumoniae* cells of monoclonal antibody P1/MCA4 against P1 (SP4 vs. SP43%Gel.) Control?

Frames were taken each 0.5 seconds of observation and are showed at 20 frames per second in the movie. The blank frame/s in the first seconds of the movie denote when the polyclonal antibodies were added to cells.

Video II. Effects on *M. pneumoniae* cells of polyclonal antibodies against P40/P90 (SP4 vs. SP43%Gel.)

Frames were taken each 0.5 seconds of observation and are showed at 20 frames per second in the movie. The blank frame/s in the first seconds of the movie denote when the polyclonal antibodies were added to cells.

Video III. Effects on *M. pneumoniae* cells of polyclonal antibodies against P1 (SP4 vs. SP43%Gel.)

Frames were taken each 0.5 seconds of observation and are showed at 20 frames per second in the movie. The blank frame/s in the first seconds of the movie denote when the polyclonal antibodies were added to cells.

Video IV. Conformational changes between open and closed forms